In vivo BiFC analysis of Y14 and NXF1 mRNA export complexes: preferential localization within and around SC35 domains

Ute Schmidt, Karsten Richter, Axel Bernhard Berger, and Peter Lichter

Division Molecular Genetics, Deutsches Krebsforschungszentrum, D-69120 Heidelberg, Germany

The bimolecular fluorescence complementation (BiFC) assay, which allows the investigation of interacting molecules in vivo, was applied to study complex formation between the splicing factor Y14 and nuclear export factor 1 (NXF1), which evidence indicates are functionally associated with nuclear mRNA. Y14 linked to the COOH terminus of yellow fluorescent protein (YFP; YC-Y14), and NXF1 fused to the NH_2 terminus of YFP (YN-NXF1) expressed in MCF7 cells yielded BiFC upon specific binding. Fluorescence accumulated within and around nuclear speckles, suggesting the involvement of speckles in mRNA processing and export. Accordingly, BiFC depended on transcription and full-length NXF1. Coimmunoprecipitation of YC-Y14 with YN-NXF1, NXF1, Y14, and RNA indicated that YC-Y14 and YN-NXF1 functionally associate with RNA. Fluorescence recovery after photobleaching and fluorescence loss in photobleaching revealed that roughly half of the accumulated BiFC complexes were immobile in vivo. This immobile fraction was readily depleted by adenosine triphosphate (ATP) administration in permeabilized cells. These results suggest that a fraction of RNA, which remains in the nucleus for several hours despite its association with splicing and export proteins, accumulates in speckles because of an ATP-dependent mechanism.

Introduction

In eukaryotic organisms, transcription is spatially separated from translation by a nuclear envelope. Consequently, gene expression requires nuclear export of mature mRNA. Although the distribution of individual mRNA export factors has been studied, as has that of several nuclear mRNAs, the use of bimolecular fluorescence complementation (BiFC) analysis makes it possible to study the in vivo formation of complexes between different export factors that evidence indicates are functionally associated with RNA. We have used this approach to study the distribution, dynamic behavior, and relationship of Y14–nuclear export factor 1 (NXF1) complexes to RNA synthesis. The assay relies on the reconstitution of fluorescent YFP by the association of two nonfluorescent YFP half-molecules, each linked to one of two proteins, whose interactions are of interest (Hu et al., 2002). Evidence indicates that many or all of the complexes visualized are associated with RNA. Thus, monitoring the interaction of Y14 and NXF1 by BiFC indirectly allows the observation of potentially export-competent mRNA. Y14 is known to bind mRNA as part of the exon–exon junction complex (EJC) at a late stage of splicing (Kataoka and Dreyfuss, 2004) and remains bound to mRNA until translation in the cytoplasm (Dostie and Dreyfuss, 2002). Bound to the EJC, NXF1 (also called TAP) promotes export of the mature mRNA (for reviews see Dreyfuss et al., 2002; Erkmann and Kutay, 2004).

We show that coexpression of the two modified proteins, YC-Y14 and YN-NXF1, carrying the COOH- and NH_2-terminal parts of YFP, respectively, allows observation of a characteristic BiFC pattern in cell nuclei. Unexpectedly, BiFC fluorescence accumulated in speckle-associated patches, suggesting an active role for speckles in mRNA processing, although they are otherwise considered mainly as storage sites for splicing and export factors (Reed and Hurt, 2002). Findings also provided insight into the idea that the nuclear retention of RNA is one way in which nature regulates gene expression. Concordantly, it had been found that only a small fraction of all transcribed RNA is exported to the cytoplasm, although most of nuclear polymerase II–derived RNA is maturely spliced and polyadenylated (Gondran et al., 1999; Jackson et al., 2000; Weil et al., 2000).

Correspondence to Peter Lichter: m.macleod@dkfz.de

Abbreviations used in this paper: BiFC, bimolecular fluorescence complementation; DRB, 5,6-dichloro-1-β-D-ribofuranosylbenzimidazole; EJC, exon–exon junction complex; FLIP, fluorescence loss in photobleaching; NXF1, nuclear export factor 1; pol II, RNA polymerase II.

The Journal of Cell Biology, Vol. 172, No. 3, January 30, 2006 373–381
http://www.jcb.org/cgi/doi/10.1083/jcb.200503061

Studies using BiFC to visualize Y14–NXF1 export complexes provide new evidence relating to the nuclear retention of mRNA in vivo.

Results

YC-Y14 and YN-NXF1 reconstitute YFP fluorescence with a characteristic nuclear distribution

Upon cotransfection of YC-Y14 and YN-NXF1, MCF7 cells emitted YFP fluorescence depending on BiFC maturation for 2 h at 30°C (Fig. 1 A). Fluorescence was observed in >90% of the cells. The signal was characterized by its nuclear localization and the composition of patchy accumulations embedded in a diffuse background. In nucleoli, the signal level was very low. Immunostaining of the YC epitope (the COOH-terminal area of YFP) essentially colocalized with the BiFC pattern (Fig. 1 A). Y14 tagged by full-length YFP displayed a similar pattern, except that it also stained nucleoli (Fig. 1 B, YFP-Y14). In contrast, patchy accumulations were less obvious with YFP-tagged NXF1, where focal accumulations aligned at the nuclear periphery appeared as a characteristic expression pattern (Fig. 1 B, YFP-NXF1).

BiFC of YFP from YC-Y14 and YN-NXF1 depends on specific interaction of the two BiFC partners

When the fusion partners YC-NXF1 and YN-Y14 were cross exchanged, YFP fluorescence was not reconstituted, even though transfection efficiency as revealed by YC immunostaining was still high (unpublished data). Furthermore, BiFC as obtained with YC-Y14 and YN-NXF1 did not occur if NXF1 was mutated by deletion of the NH_2-terminal 60 or 371 amino acids (Fig. 1, C and D). Deletion of the first 60 amino acids of NXF1, which are known to interact with the EJC protein E1B-AP5 (Bachi et al., 2000), is supposed to prevent BIFC formation caused by disturbed interaction with Y14, whereas the deletion of the NH_2-terminal 371 amino acids totally compromises interaction with RNA (Braun et al., 1999; Bachi et al., 2000; Liker et al., 2000). With both mutations, BiFC occurred in <10% of the cells, even though transfection efficiency was >90%, as determined by YC immunodetection, and the nuclear distribution, which was monitored by full YFP tags (YFP-NXF1 Δ1–371 and YFP-NXF1 Δ1–60), was not seemingly influenced by the mutation (Fig. 1 B). In the few cases of BiFC, fluorescence was very weak and different from the characteristic patchy pattern of BiFC with full-length NXF1. In particular, BiFC with YN-NXF1 Δ1–371 only occurred in cells with shrunken nuclei and abnormally condensed chromatin.

Do YC-Y14 and YN-NXF1 functionally interact with RNA?

The aforementioned experiments support the hypothesis that functional interaction of the proteins YC-Y14 and YN-NXF1 is a prerequisite for the reconstitution of fluorescent YFP. As such, BiFC should depend on active mRNA transcription. Accordingly, BiFC was compromised upon RNA polymerase II (pol II) inhibition with either 5,6-dichloro-1-β-D-ribofuranosylbenzimidazole (DRB) or α-amanitin at 37°C, even though expression of the YC epitope still appeared unperturbed (Fig. 2 A; α-amanitin not

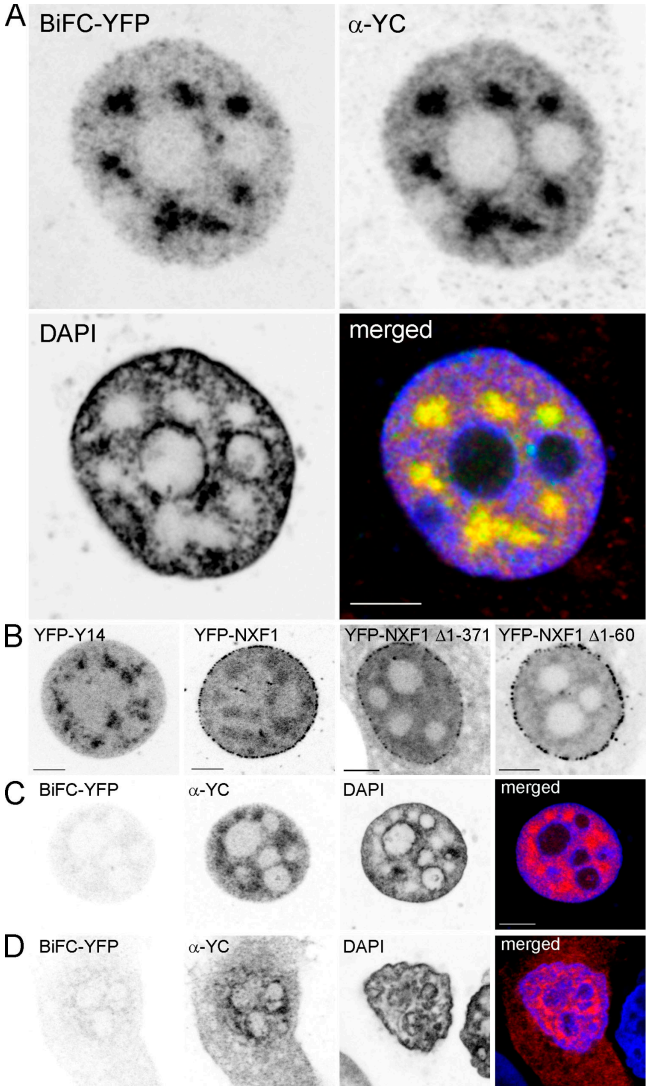

Figure 1. **BiFC of YFP from YC-Y14 and YN-NXF1 depends on specific interaction of the NXF1 and Y14 moieties.** (A) MCF7 cells transfected with YC-Y14 and YN-NXF1 were incubated for 2 h at 30°C for BiFC maturation. BiFC signals are shown in the top left image. Distribution of the YC epitope in the same cell was revealed by α-YC immunodetection (top right), and chromatin was stained by DAPI (bottom left). BiFC of YFP from YN-NXF1 and YC-Y14 was confined to nuclei, where it formed a patchy pattern in chromatin-poor regions, excluding nucleoli. YFP fluorescence by BiFC and immunodetection of YC-Y14 did correspond to each other (merged; bottom right). (B) YFP-Y14 (left) corresponded to the BiFC pattern, except that nucleoli were also labeled. In contrast, YFP-NXF1 (middle left) showed focal accumulations aligned at the nuclear periphery, whereas the accumulation in specklelike patches was less conspicuous because of a higher background of inhomogeneous signal throughout the nucleus. Deletion of part of the NH_2 terminus in NXF1 did not seriously alter the distribution of the protein. In particular, both deletion mutations (NXF1 Δ1–60 and NXF1 Δ1–371) localized to the nucleus and formed focal accumulations aligned at the nuclear periphery (middle right and right). (C and D) MCF7 cells, cotransfected with either YC-Y14–YN-NXF1 Δ1–371 (C) or YC-Y14–NXF1 Δ1–60 (D), were incubated for 2 h at 30°C for BiFC maturation. Without deletions, the BiFC pattern that is characteristic for full-length constructs was not observed. Merged images: red, α-YC; green, YFP; blue, DAPI. Bars, 5 μm.

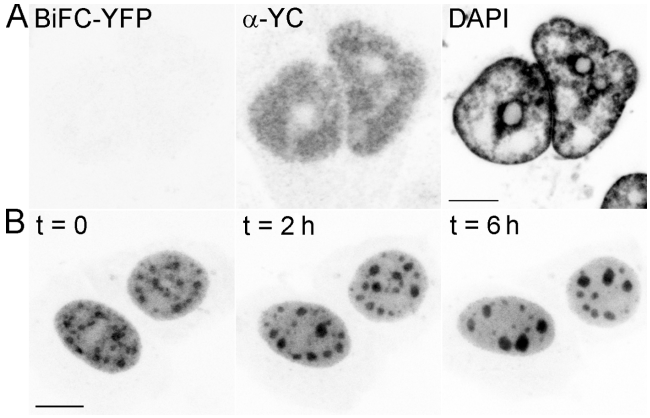

Figure 2. **BiFC of YFP from YC-Y14 and YN-NXF1 depends on pol II activity during BiFC maturation.** (A) Pol II inhibition by DRB at 37°C compromises subsequent BiFC maturation at 30°C (left), even though the expression level of proteins appears unperturbed (middle, YC immunodetection in identical cells; right, DAPI image). (B) Pol II inhibition by DRB at 30°C after maturation of BiFC did not abolish the already established BiFC signal. DRB treatment caused BiFC patches to gather and fuse into larger particles over time (duration of DRB incubation as indicated), which is a behavior already described for SC35 domains (Spector et al., 1991). Bars, 5 μm.

depicted). In contrast, pol II inhibition after BiFC maturation at 30°C did not abolish the signal, which remained stable within 5% for a period of at least 6 h (Fig. 2 B). Immunoprecipitation of YC-Y14 in nuclear extracts of BiFC-matured cells confirmed the expected interactions. Targeted against the YC epitope of YC-Y14, immunoprecipitation coprecipitated YN-NXF1, NXF1, Y14, and radiolabeled RNA (Fig. 3).

BiFC patches colocalize with SC35 domains and the perispeckle region

Signal patches of BiFC from YC-Y14 and YN-NXF1 resembled speckles in respect to size, shape, and number. Speckles are nuclear bodies enriched in splicing and export factors (Spector, 1990; Zhou et al., 2000; Rodrigues et al., 2001). Colocalization of the BiFC patches with speckles was investigated by immunodetection of SC35, a marker protein for speckles (Fig. 4). All BiFC patches colocalized with SC35 domains, and vice versa. However, the BiFC patches were larger than their corresponding SC35 domain, surmounting the speckle perimeter by up to 500 nm. In ~10% of the cells, the perispeckle signal was even higher than the SC35-positive center.

Export of BiFC complexes partially depends on ATP

Export capability of the BiFC complexes was investigated in digitonin-permeabilized cells. Permeabilization allows observation of unidirectional nuclear export (Kehlenbach, 2003) because soluble factors necessary for reimport become depleted. Upon permeabilization, the whole nuclear level of BiFC fluorescence decreased by two thirds within 5 min (Fig. 5 A) and remained stable for at least 5 min further. However, the remaining YFP fluorescence was immediately extinguished upon administration of 5 mM ATP. To further verify the role of ATP in releasing the Y14–NXF1 complexes, cells were pretreated with

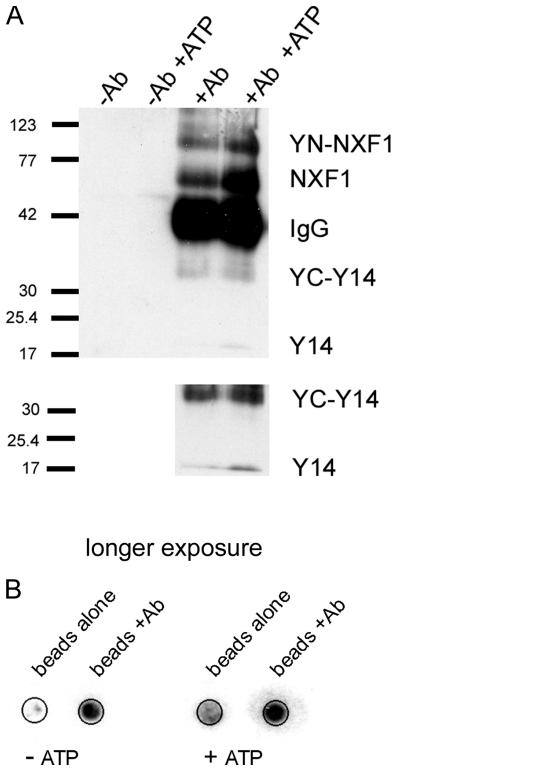

Figure 3. **YC-Y14 forms complexes with Y14, YN-NXF1, NXF1, and RNA.** (A) Immunoprecipitation of YC-Y14 from the nucleoplasmic fraction of BiFC-matured MCF7 cells coprecipitated YN-NXF1, as well as endogenous NXF1 and Y14. Addition of ATP to the buffer did not dissociate the complexes. (bottom) Prolonged exposure of the same blot. (B) Immunoprecipitation of YC-Y14 from the nucleoplasmic fraction of BiFC-matured cells coprecipitated radiolabeled RNA. In contrast to proteins, the beads used for immunoprecipitation bind RNA without antibody coating. As shown by the mock control (beads alone), this false positive background was low compared with the amount of coprecipitated RNA. ATP administration did not dissociate RNA from YC-Y14.

sodium azide to deplete cellular levels of ATP. Sodium azide treatment reduced overall BiFC intensity. In particular, the diffuse background appeared extracted and a diffuse rim emerged at the nuclear periphery. Upon digitonin permeabilization, the signal level decreased by 50%. Again, the administration of 5 mM ATP caused the complete loss of fluorescence (Fig. 5 B).

Short-term immobile fractions of BiFC complexes slowly turn over in living cells

To measure immobile fractions and the recovery speed of BiFC complexes in speckles and the nonspeckle nucleoplasm, FRAP was performed within 2-μm-diam circular regions of interest (Fig. 6). Immobile fractions measured by FRAP were confirmed by fluorescence loss in photobleaching (FLIP; Table I). Because temperature dependence was of special concern in this study, FRAP was also measured for YFP-Y14 to observe a possible shift from 37 to 30°C and RT (Table I). Besides a marginal trend of decreased immobile fraction in the cold, temperature had no significant effect within the error of individual measurements. For the BiFC signal, immobile fractions were much higher in speckles (46%) than in the nonspeckle nucleoplasm (21%). In contrast, recovery time of the mobile fraction was

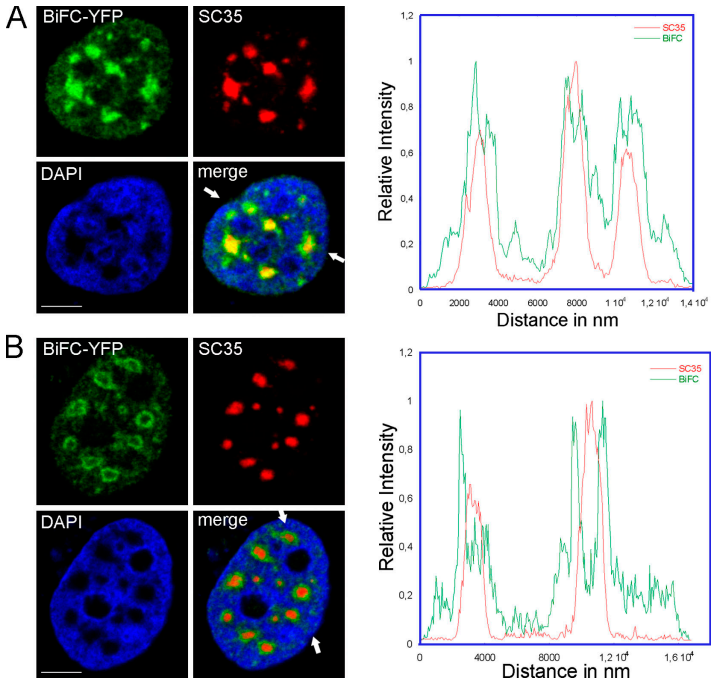

Figure 4. **BiFC-labeled Y14–NXF1 complexes accumulate in speckles and a perispeckle region.** Immunolocalization of speckles (anti-SC35) in MCF7 cells, which express BiFC-YFP from YC-Y14 and YN-NXF1. (A) All BiFC patches always colocalize with speckles, and vice versa. All BiFC patches surmount their corresponding speckles in size (green border in merged image). Arrows indicate the position of a line scan across three speckles. (B) In ∼10% of BiFC-expressing cells, the perispeckle BiFC signal was even stronger than the signal over the speckle. Line scan across two speckles. Red, anti-SC35; green, BiFC-YFP; blue, DAPI-labeled chromatin. Bars, 5 μm.

similar in both compartments (1.6 s). Sodium azide treatment significantly increased the immobile fractions (74 and 55%) and also decreased the recovery times. In particular, fluorescence recovery was much slower in speckles compared with the nonspeckle nucleoplasm (Table I). Performed in a timescale of 35 s, FRAP measured the mobility of fluorochromes already established at the time of bleaching. Bleaching all fluorescence of the complete nucleus, in contrast, allowed observation of de novo BiFC formation (Fig. 6). It took roughly 2 h for a steady state of restoration, which resembled the initial state. Separate analysis of the time course of recovery within speckles and the nonspeckle nucleoplasm revealed that speckles reached only 80% of their initial value.

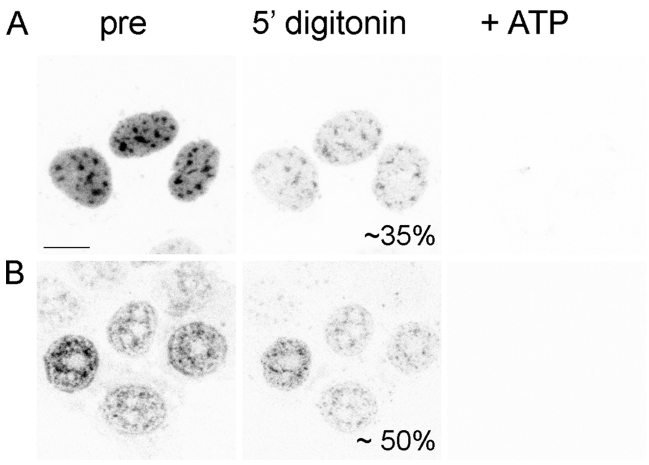

Figure 5. **Depletion of BiFC-YFP upon ATP administration.** (A) Upon selective permeabilization of the cell membrane by digitonin, the initial BiFC fluorescence level (left) decreased by roughly 65% (middle). The remaining fluorescence vanished within seconds upon administration of 5 mM ATP (right). (B) Sodium azide treatment reduced overall BiFC intensity, and a diffuse stain at the nuclear periphery became prominent (left). In these cells, the initial signal level diminished by 50% upon digitonin permeabilization without ATP (middle). Complete loss of fluorescence could also be triggered by the administration of 5 mM ATP (right). Bar, 10 μm.

Discussion

Recently, in vivo analysis of nuclear mRNA greatly contributed to our current understanding of RNA dynamics. However, measuring the dynamics of processed endogenous mRNA in vivo has been challenging. Studies that visualize mRNA export factors individually cannot distinguish functionally associated reporters from unbound reporters. We used the BiFC approach to visualize the interaction of Y14 and NXF1. Furthermore, evidence indicates that these complexes are associated with nuclear RNA. Thus, monitoring the interaction of target molecules instead of labeling single molecules by fluorescent protein tags or by FISH probes allows discrimination of false positive backgrounds from noninteracting entities. Compared with fluorescence resonance energy transfer, which is another method used to visualize protein–protein interaction in situ, the signal-to-noise ratio is higher in the BiFC experiments because the signal is measured directly. In contrast, fluorescence resonance energy transfer analysis requires cross talk compensation between donor and acceptor channels, which intrinsically increases statistical noise.

As NXF1 binds to processed mRNA and mediates the interactions of the export complex with the nuclear pore complex, it is considered a mRNA export receptor (Katahira et al., 1999; Bachi et al., 2000; Herold et al., 2001). The combination of the splicing-associated protein Y14 with NXF1 was thought to label spliced mRNA with putative export capacity. BiFC from YC-Y14 and YN-NXF1 reproducibly demonstrated a specific

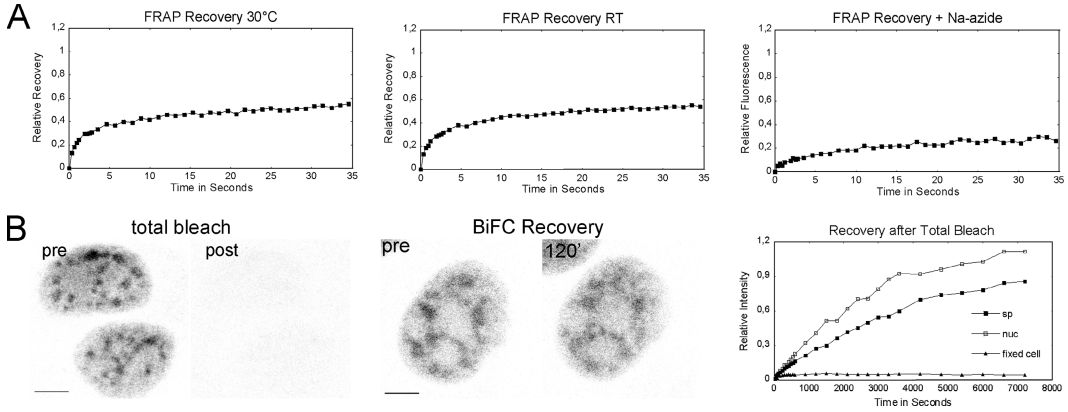

Figure 6. **A substantial amount of BiFC complexes are immobile in vivo.** The immobile fraction and half-life recovery upon photobleaching was measured within 2-μm-diam circular regions of interest that were centered over speckles and the nonspeckle nucleoplasm. (A) The FRAP curves shown were cumulated over $n = 10–15$ single measurements. Differences between measurements at 30°C and RT were not significant (Table I). Sodium azide treatment significantly increased the immobile fractions (74 and 55%) and slowed down recovery time. (B) Recovery of fluorescence by de novo maturation of BiFC was observed after bleaching all fluorescence of the complete nucleus (left, maximum projection of nuclei before and immediately after total bleach). 2 h after total bleach, the initial BiFC signal was almost restored (middle, images of the same nucleus before total bleach and 120 min after bleach). The time course of fluorescence intensity measured separately over speckles and the nonspeckle nucleoplasm reveals that recovery reached only 80% of its initial value (right). Control measurement in fixed cells demonstrates 5% curing of the bleached fluorochromes. Bars, 5 μm.

nuclear distribution of the interacting proteins, revealing spatial association with the speckle compartment in particular.

The BiFC approach is particularly well suited for in vivo observations. A peculiar requirement is the maturation at a low temperature (30°C). Because cells still grow and divide at this temperature, mRNA processing and export go on at physiologically acceptable rates. Accordingly, even though we observed a trend in reduction of the immobile fraction of YFP-Y14 in speckle-associated patches, temperature dependence of immobile fractions and recovery times upon photobleaching were not significant. Thus, we consider the shift to 30°C of marginal influence on the analysis of RNA maintenance by the BiFC assay.

Several experiments were performed to demonstrate that the BiFC assay labels functional interaction of the two proteins with RNA. First, the cross exchanged pair YN-Y14–YC-NXF1 did not reconstitute YFP, indicating that BiFC depended on the sterical configuration of the linked proteins, Y14 and NXF1, and that the YC and YN parts did not interact in solution to reconstitute fluorescence. Second, the characteristic BiFC pattern was not observed if the NH_2-terminal 60 or 371 amino acids of NXF1 were deleted, even though topological expression of the proteins was not affected. The NH_2-terminal part of NXF1 is responsible for RNA binding and interaction with the EJC (Braun et al., 1999; Bachi et al., 2000; Liker et al., 2000). According to Bachi et al. (2000), deletion of the first 371 amino acids blocks nuclear export and impairs viability of the cells. This may explain the bad condition of many cells transfected with YN-NXF1 Δ1–371. BiFC fluorescence, with YN-NXF1 Δ1–371 exclusively seen in shrunken nuclei, may have evolved because of aggregation of the BiFC chimeras. The first 60 amino acids are involved in interaction of NXF1 with the EJC protein E1B-AP5 (Bachi et al., 2000). Because NXF1 Δ1–60 still binds to RNA (Braun et al., 1999, 2001), interaction of YN-NXF1 with YC-Y14 may occur with low efficiency, explaining the few cases where BiFC fluorescence could be monitored, although at

Table I. **Mobility of BiFC complexes and YFP-Y14 in MCF7 cell nuclei**

	Half-life recoveries		Immobile fraction	
	Speckle	Nucleoplasm	Speckle	Nucleoplasm
	s	*s*	%	%
FRAP				
YFP-Y14 37°C	0.26 (0.26/0.3)	0.25 (0.28/0.24)	36 (27/40)	12 (9/19)
YFP-Y14 30°C	0.28 (0.26/0.3)	0.25 (0.24/0.29)	33 (29/37)	13 (5/21)
YFP-Y14 RT	0.26 (0.26/0.26)	0.25 (0.23/0.26)	29 (27/33)	17 (14/20)
BiFC 30°C	1.6 (1.3/2.1)	1.3 (1.0/2.1)	47 (43/49)	22 (17/31)
BiFC RT	1.9 (1.1/2.1)	1.5 (1.2/1.8)	46 (42/50)	20 (12/27)
BiFC + sodium azide	3.7 (3.2/4.5)	2.5 (2.3/4.1)	74 (72/75)	55 (43/66)
FLIP				
BiFC 30°C	-	-	43 (31/53)	23 (17/30)
BiFC RT	-	-	34 (30/44)	20 (17/25)

Of $n = 10–15$ acquired values, the ranked mean is shown together with the third/ninth value in parentheses.

very low intensity. Third, immunoprecipitation of YC-Y14 from nuclear extracts not only coprecipitated YN-NXF1 but also Y14, NXF1, and radiolabeled RNA, demonstrating that all expected interactions of YC-Y14 did occur. In particular, this experiment shows directly that the YC tag does not prohibit interaction with NXF1. Fourth, BiFC from YC-Y14 and YN-NXF1 requires pol II activity. Inhibition of pol II by DRB or α-amanitin before BiFC maturation prohibited fluorescence reconstitution, whereas already established fluorescence was not affected by pol II inhibition. All together, these experiments suggest that BiFC of YFP from YC-Y14 and YN-NXF1 monitors endogenous mRNA at a terminal state of maturation.

Because BiFC-YFP represents the interaction of YC-Y14 and YN-NXF1, the characteristic BiFC pattern should be part of both YFP-Y14 and YFP-NXF1 distributions. This was the case, as both constructs showed nuclear location with accumulation in specklelike patches. Differences from the characteristic BiFC pattern may be attributable to entities that are not functionally associated with RNA, such as the nucleolar localization of YFP-Y14. The focal accumulations of YFP-NXF1 at the nuclear edge may represent cytoplasmic entities that become docked to nuclear pores before import (Forler et al., 2004).

The BiFC complexes accumulated within speckles and the perispeckle region, suggesting a functional role of the speckle compartment in mRNA processing, including maturation and/or transport. Furthermore, the pronounced enrichment of BiFC complexes in the perispeckle space indicates that speckles associate with a specific nuclear environment.

The accumulation of RNA in speckles had already been observed for both microinjected and endogenous RNA that were labeled by FISH with either an oligo d(T) probe or sequence-specific probes (Carter et al., 1991; Zirbel et al., 1993; Melcak et al., 2001; Shopland et al., 2002). Because BiFC has a maturation time that is >2 h (Hu and Kerppola, 2003), the observed accumulation in speckles derives from complexes of rather long nuclear residence time. The poor mobility of BiFC complexes was experimentally revealed by FRAP and FLIP and was further confirmed in cell permeabilization assays. Upon cell permeabilization, roughly two-thirds of the BiFC signal was eluted. The remaining fluorescence of an apparently immobile fraction completely disappeared upon administration of ATP. One might argue that ATP destroys the BiFC complexes. However, YN-NXF1 still coprecipitates with YC-Y14 upon ATP administration, indicating that the effect of ATP is the release of the complexes. ATP-dependent mobilization of splicing- and export-related factors were described for the alternate splicing factor (Misteli et al., 1997) and the EJC protein SRm160 (Wagner et al., 2004). ATP-dependent export was also observed for in vitro–transcribed rab11 mRNA (Ossareh-Nazari et al., 2000).

In cells treated with sodium azide, the diffuse background of BiFC complexes strongly decreased. The speckle-associated accumulations became more prominent, and a rim emerged at the nuclear periphery. This reorganization may be caused by the extraction of a soluble part of BiFC complexes or by the reduced release of bound complexes. Accordingly, a lower fraction of fluorescence was eluted upon digitonin permeabilization. The peripheral rim was broad and not sharply delimited, unlike the focal accumulations of NXF1. It may represent a zone of weak binding for mRNA, which only becomes visible when the diffuse background of presumptively mobile BiFC complexes disappeared.

In vivo analysis of mobility by FRAP was kept simple. Half-life recovery and immobile fractions were read out directly from the recovery plots of bleach-corrected raw data. Neither curve fitting to decipher the complexity of presumptively superposed events nor modeling of diffusion constants wer performed. Thus, the data presented are valuable for direct comparison only. Recovery of YFP-Y14 was faster, compared with BiFC-YFP. Because the YFP-Y14 signal does not represent a pure population of complexed molecules, a fraction of unbound molecules will account for this apparent faster mobility. One might also argue that BiFC formation, by itself, impedes mobility of the complexes.

Measured by FRAP or FLIP, roughly half of the BiFC-forming complexes in the speckle-associated patches were immobile, and the immobile fraction was lower in the nonspeckle nucleoplasm, suggesting a functional association of BiFC complexes with speckles. Further evidence for functional association with speckles compared with haphazard immobilization caused by the artificial BiFC tag is provided by the efficient release of immobile BiFC complexes upon ATP administration in permeabilized cells.

Upon incubation of cells in sodium azide, most of the BiFC signal became immobile. According to the ATP-dependent release in permeabilized cells, ATP depletion may have impaired the release of bound complexes rather than decreased the nuclear export rate. FRAP of diffusible molecules is a fast process. In our study, an approximately steady state was reached within a period of 35 s. In contrast, bleaching the entire pool of fluorescence in a cell allows the observation of fluorescence turnover instead of diffusion. Upon total bleach of a nucleus, the initial BiFC pattern recovered within a period of ∼2 h, demonstrating its turnover even within BiFC patches.

Previous studies reported that speckles contain poly(A) RNA (Carter et al., 1991; Huang et al., 1994). As shown by Johnson et al. (2000) and Shopland et al. (2002), at least part of this speckle RNA comes from transcription of protein-coding genes. Although possibly all actively transcribed genes associate with the surface of speckles (Huang and Spector, 1991; Johnson et al., 2000), some genes' interaction with speckles is particularly intimate, as their transcription products pervade the associated speckle ("typeI genes;" Smith et al., 1999). Transcripts can even move over and accumulate in the entire speckle compartment of the nucleus (Hattinger et al., 2002). Enrichment of messengers in speckles, however, appears to depend on the particular conditions of either the cell state or the transcript. Thus, observable accumulation throughout the entire speckle compartment of the induced gene p21 transcripts occurred in <20% of the induced cells (Hattinger et al., 2002). Comparing the distribution of collagen 1α1 and 1α2 transcripts in cultured fibroblast nuclei, Shopland et al. (2002) found significant different distribution patterns. The collagen 1α1 product pervades the entire associated speckle. Because transcripts of a splice mutation of collagen 1α1 that never leave the nucleus also

pervade the entire associated speckle (Johnson et al., 2000), one may argue that speckle-associated mRNA is retained before export. This also explains why their prevalence remains practically stable upon transcripition inhibition (Huang et al., 1994; Shopland et al., 2002). Long residence time is also a characteristic feature of the observed BiFC complexes because of the duration of fluorescence maturation. There may be complexes that exit the nucleus quicker. These, however, would not be visible by the assay, as the complex is supposed to decay in the cytoplasm. Although we cannot exclude the possibility that the BiFC complexes are artificially bound within speckles because of their tag, they may equally represent a fraction of normally retained RNA. In any case, the assay reveals a possible involvement of the speckle-associated nuclear space in retention of processed mRNA.

BiFC of YFP from YC-Y14 and YN-NXF1 indicates that mammalian cell nuclei harbor NXF1-associated mRNA with very long residence times, implying that association of RNA with NXF1 is insufficient for immediate export. Because the BiFC signal can be released by ATP, an ATP-dependent mechanism may be involved in the export prohibition of NXF1-associated RNA.

Materials and methods

Plasmid construction
Full-length NXF1 and Y14 sequences were PCR amplified and cloned into peYFP-C1 (CLONTECH Laboratories) using EcoRI–BamHI (New England BioLabs, Inc.) restriction sites. Subsequently, the eYFP was substituted by the 1–154 or the 155–238 fragment of eYFP. These fragments were PCR amplified and inserted using AgeI–XhoI or AgeI–BspEI (New England BioLabs, Inc.) restriction enzymes to generate fusion proteins with the NH_2- or COOH-terminal parts of YFP (YN-NXF1, YN-Y14, YC-NXF1, and YC-Y14, respectively). NXF1 deletion mutants (YN-NXF1 Δ1–60 and YN-NXF1 Δ1–371) were linked to full-length YFP or to the NH_2-terminal part of YFP using EcoRI–BamHI.

Single transfection of the plasmids used for BiFC (YN-x and YC-x) did not produce fluorescence, indicating that the vectors did not code for full-length YFP.

Cell culture
Human MCF7 cells were cultured in DME supplemented with 10% FCS. 1 d before transfection, cells were seeded onto coverslips or in Lab-Tek chambers (Nunc) and transfected using Effectene (QIAGEN) according to the manufacturer's instructions. 16–48 h after transfection, cells were washed with PBS and incubated with fresh medium at 30°C for at least 2 h to allow fluorophore maturation. Live cell observations were performed in DME containing 20 mM Hepes, pH 7.0 on a heating stage.

For ^{32}P labeling of RNA (Lerner and Steitz, 1979), cells were washed with prewarmed, phosphate-free DME (Invitrogen) and incubated with 0.4 mCi ^{32}P (GE Healthcare) per 200 ml of phosphate-free DME supplemented with 50 mM Hepes (Invitrogen) for 4 h at 30°C.

Immunofluorescence
Cells were fixed with 4% formaldehyde in PBS with 2% sucrose for 15 min on ice, permeabilized in 0.2% Triton X-100 for 3 min on ice, preincubated with 4% goat serum for 10 min at RT, and incubated with primary antibody (mouse α-SC35; Sigma-Aldrich; rabbit α-GFP; Abcam pvc) for 30 min at 37°C. The GFP antibody cross reacts with the YC epitope. Samples were washed and incubated with Cy5-labeled secondary antibodies (Dianova) for 30 min at 37°C. Coverslips were mounted with Vectashield containing DAPI (Linaris) for direct observation.

Transcription inhibition and energy starvation
Pol II transcription was inhibited by incubation in 50 μg/ml DRB or α-amanitin in DME for 6 h. For energy starvation, cells were incubated for 20 min at 30°C in PBS containing 10 mM sodium azide, 50 mM of deoxy-glucose, 1 mM $MgCl_2$, and 0.5 mM $CaCl_2$ (Svitkina and Borisy, 1999).

Cell permeabilization assay
For selective permeabilization of the cell membrane, unfixed cells were incubated for 5 min at 30°C with 40 μg/ml digitonin (Calbiochem) in transcription buffer (Stanek et al., 2000), following the protocol used by Adam et al. (1990). In experiments with ATP supply after permeabilization, digitonin was replaced by transcription buffer containing 5 mM ATP.

Cell fractionation, coimmunoprecipitation, and Western blotting
Transfected cells were trypsinized, suspended in prewarmed DME, and washed with ice-cold PBS. For the cytoplasmic preparation, the cell membrane was permeabilized for 5 min on ice with digitonin buffer supplemented with complete EDTA-free protease inhibitor cocktail (Roche), 0.1 mM PMSF (Sigma-Aldrich), and 250 mM KCl. Cells were spun down at 800 *g* for 3 min, the supernatant was taken off, and cells were respun at 15,000 *g* and saved. The pellet containing the nuclear fraction was resuspended in buffer containing 0.1% NP-40, incubated on ice for 10 min, and spun at 15,000 *g* for 3 min, and the supernatant was saved.

For immunoprecipitation, 200-μl protein A–Sepharose beads (GE Healthcare) were washed in NP-40 buffer and blocked with 100 μg/ml of *Escherichia coli* tRNA and 1 mg/ml BSA. Beads were incubated with antibody (α-GFP; Abcam pvc) at a ratio of 20:1 for 1 h, in a total volume of 500 μl. Cell extracts were incubated with either antibody-coated beads or beads alone overnight. Beads were washed three times in 1 ml of buffer and resuspended in 300 μl of buffer. All steps were performed at 4°C. Proteins were isolated from the beads and denatured by boiling in Laemmli buffer (2% SDS, 20% glycerol, 20 mM Tris-Cl, pH 8, 2 mM EDTA, 1 mM DTT, and 0.1 mg/ml Bromophenol blue) for 5 min.

For Western blotting, proteins were separated by 10% SDS-PAGE, transferred to a PVDF membrane (Millipore), and detected with rabbit α-NXF1 (gift from E. Hurt, University of Heidelberg, Heidelberg, Germany), rabbit α-GFP (Abcam pvc), or mouse α-Y14 (Abcam pvc). The secondary antibodies used were α-rabbit–HRP and α-mouse–HRP (DakoCytomation).

RNA purification with TRIzol
After the immunoprecipitation, 1 ml TRIzol (Invitrogen) was added, mixed, and incubated at RT for 5 min. 200 μl chloroform was added, mixed, and incubated at RT for 15 min. Phases were separated by centrifugation at 15,000 *g* for 5 min. The upper phase was saved, 10 μg of glycogen was added, and RNA was precipitated with 500 μl isopropanol. The pellet was washed with 70% ethanol, resuspendend in 5 μl of nuclease-free water, and spotted onto a nitrocellulose membrane. Radioactivity was exposed on BioMax MS film (Kodak).

Confocal laser scanning microscopy and image processing
Fluorescence images were acquired by confocal laser scanning microscopy (model TCS SP2; Leica) with a 63×, NA 1.32, oil objective at pinhole size 1 Airy and a nominal voxel size of 58 × 58 × 284 nm^3. DAPI, YFP, and Cy5 were excited by 405-, 514-, and 633-nm laser light and emission was detected at 410–500, 520–590, and 640–700 nm, respectively. Cross talk was minimized by serial acquisition of the fluorescence color channels. The digital images were analyzed with either LSM software (Leica) or analySIS pro 3.2 (Soft Imaging System GmBH). All micrographs in Fig. 5 have been deconvoluted (blind three dimensional) with analySIS pro 3.2. Frequency distributions of intensities were collected either over a regions of interest or through binary masks, which were configured by global thresholding, morphologic filtering, and interactive editing. Two features of interest were compared, which were the BiFC signal in speckles (corresponding to the SC35 domains), including a perispeckle compartment and the nuclear area, except for speckles and nucleoli. Note that the "nonspeckle nucleoplasm" is heterogeneous, as it contains chromatin, nuclear bodies, and parts of the speckle compartment that were not identified as speckles.

FRAP
FRAP was performed in two dimensions within the bleach zones of a 2-μm nominal diam positioned over speckles and the nonspeckle nucleoplasm. Image size was 64 × 256 pixels at a lateral pixel size of 116 nm. Lag time between bleaching and the first recovery measurement was 0.625 ms at a line rate of 800 Hz. Beam expander of the illumination path was set to value 1 and the pinhole to 6 Airy.

Four postbleach images were taken every 107 ms, followed by four images every 214 ms and 30 images every 1.07 s. The period of

recovery measurement was adjusted to reach saturation (up to 100 s). After subtraction of the mean of image black level, the recovery data were corrected for FLIP effects and postbleach loss of fluorescence during recovery observation and transformed into relative values according to $I_{rel} = I_t/I_0 \times T_0/T_t$, with I_0 being the initial intensity and I_t the intensity at the time t in the bleached spot, and T_0 and T_t being the total nuclear intensity before bleach and at time t, respectively. Immobile fractions and the period to reach half saturation (half-life) were directly read out from plotted FRAP curves.

FLIP

For FLIP analysis, approximately one half of a cell nucleus was bleached 100 times every 1.6 s at maximum laser intensity and beam expander 1 while the unbleached part of the nucleus was not illuminated.Two dimensional image acquisition before and after bleaching was conducted with pinhole size 6 Airy. For data analysis, the black level was subtracted and the postbleach image corrected for observation-induced bleaching. The factor for bleach correction was calculated from the fluorescence decay, I_t/I_0, of an adjacent unbleached cell observed under the same conditions.

Recovery of BiFC after total bleach of the cell nucleus

A complete loss of fluorescence across the entire cell nucleus was achieved with 25 repeated scans at maximum laser intensity. Fluorescence recovery was then observed over 2 h, and images of the same confocal plane were recorded 4 times every 30 s, followed by 8 times every 1 min, 10 times every 5 min, and 6 times every 10 min. The images were black level subtracted and the time-dependent increase in intensity was measured as mean intensity through masks designed for speckles and the nonspeckle nucleoplasm.

The support of Tom Kerppola and Malte Wachsmuth is gratefully acknowledged. We would like to thank Harald Herrmann and Daniel Mertens for constructive suggestions. We are grateful to Ed Hurt for providing antibodies against human NXF1/TAP. Katalin Fejes Tóth, Michelle Nessling, Don and Ada Olins, and Tamás Fischer are gratefully acknowledged for critical reading of the manuscript and valuable discussions. We also thank Roland Eils for the use of his microscope imaging device.

Submitted: 11 March 2005
Accepted: 22 December 2005

References

Adam, S.A., R.S. Marr, and L. Gerace. 1990. Nuclear protein import in permeabilized mammalian cells requires soluble cytoplasmic factors. *J. Cell Biol.* 111:807–816.

Bachi, A., I.C. Braun, J.P. Rodrigues, N. Pante, K. Ribbeck, C. von Kobbe, U. Kutay, M. Wilm, D. Gorlich, M. Carmo-Fonseca, and E. Izaurralde. 2000. The C-terminal domain of TAP interacts with the nuclear pore complex and promotes export of specific CTE-bearing RNA substrates. *RNA*. 6:136–158.

Braun, I.C., E. Rohrbach, C. Schmitt, and E. Izaurralde. 1999. TAP binds to the constitutive transport element (CTE) through a novel RNA-binding motif that is sufficient to promote CTE-dependent RNA export from the nucleus. *EMBO J.* 18:1953–1965.

Braun, I.C., A. Herold, M. Rode, E. Conti, and E. Izaurralde. 2001. Overexpression of TAP/p15 heterodimers bypasses nuclear retention and stimulates nuclear mRNA export. *J. Biol. Chem.* 276:20536–20543.

Carter, K.C., K.L. Taneja, and J.B. Lawrence. 1991. Discrete nuclear domains of poly(A) RNA and their relationship to the functional organization of the nucleus. *J. Cell Biol.* 115:1191–1202.

Dostie, J., and G. Dreyfuss. 2002. Translation is required to remove Y14 from mRNAs in the cytoplasm. *Curr. Biol.* 12:1060–1067.

Dreyfuss, G., V.N. Kim, and N. Kataoka. 2002. Messenger-RNA-binding proteins and the messages they carry. *Nat. Rev. Mol. Cell Biol.* 3:195–205.

Erkmann, J.A., and U. Kutay. 2004. Nuclear export of mRNA: from the site of transcription to the cytoplasm. *Exp. Cell Res.* 296:12–20.

Forler, D., G. Rabut, F.D. Ciccarelli, A. Herold, T. Kocher, R. Niggeweg, P. Bork, J. Ellenberg, and E. Izaurralde. 2004. RanBP2/Nup358 provides a major binding site for NXF1-p15 dimers at the nuclear pore complex and functions in nuclear mRNA export. *Mol. Cell. Biol.* 24:1155–1167.

Gehring, N.H., G. Neu-Yilik, T. Schell, M.W. Hentze, and A.E. Kulozik. 2003. Y14 and hUpf3b form an NMD-activating complex. *Mol. Cell.* 11:939–949.

Gondran, P., F. Amiot, D. Weil, and F. Dautry. 1999. Accumulation of mature mRNA in the nuclear fraction of mammalian cells. *FEBS Lett.* 458:324–328.

Hattinger, C.M., A.G. Jochemsen, H.J. Tanke, and R.W. Dirks. 2002. Induction of p21 mRNA synthesis after short-wavelength UV light visualized in individual cells by RNA FISH. *J. Histochem. Cytochem.* 50:81–89.

Herold, A., T. Klymenko, and E. Izaurralde. 2001. NXF1/p15 heterodimers are essential for mRNA nuclear export in *Drosophila*. *RNA*. 7:1768–1780.

Hu, C.D., and T.K. Kerppola. 2003. Simultaneous visualization of multiple protein interactions in living cells using multicolor fluorescence complementation analysis. *Nat. Biotechnol.* 21:539–545.

Hu, C.D., Y. Chinenov, and T.K. Kerppola. 2002. Visualization of interactions among bZIP and Rel family proteins in living cells using bimolecular fluorescence complementation. *Mol. Cell.* 9:789–798.

Huang, S., and D.L. Spector. 1991. Nascent pre-mRNA transcripts are associated with nuclear regions enriched in splicing factors. *Genes Dev.* 5:2288–2302.

Huang, S., T.J. Deerink, M.H. Ellisman, and D.L. Spector. 1994. In vivo analysis of the stability and transport of nuclear poly(A)$^+$ RNA. *J. Cell Biol.* 126:877–899.

Jackson, D.A., A. Pombo, and F. Iborra. 2000. The balance sheet for transcription: an analysis of nuclear RNA metabolism in mammalian cells. *FASEB J.* 14:242–254.

Johnson, C., D. Primorac, M. McKinstry, J. McNeil, D. Rowe, and J.B. Lawrence. 2000. Tracking COL1A1 RNA in osteogenesis imperfecta: splice-defective transcripts initiate transport from gene but are retained within the SC35 domain. *J. Cell Biol.* 150:417–431.

Katahira, J., K. Strasser, A. Podtelejnikov, M. Mann, J.U. Jung, and E. Hurt. 1999. The Mex67p-mediated nuclear mRNA export pathway is conserved from yeast to human. *EMBO J.* 18:2593–2609.

Kataoka, N., and G. Dreyfuss. 2004. A simple whole cell lysate system for in vitro splicing reveals a stepwise assembly of the exon-exon junction complex. *J. Biol. Chem.* 279:7009–7013.

Kehlenbach, R.H. 2003. In vitro analysis of nuclear mRNA export using molecular beacons for target detection. *Nucleic Acids Res.* 31:e64.

Lerner, M.R., and J.A. Steitz. 1979. Antibodies to small nuclear RNAs complexed with proteins are produced by patients with systemic lupus erythematosus. *Proc. Natl. Acad. Sci. USA*. 76:5495–5499.

Liker, E., E. Fernandez, E. Izaurralde, and E. Conti. 2000. The structure of the mRNA export factor TAP reveals a cis arrangement of a non-canonical RNP domain and an LRR domain. *EMBO J.* 19:5587–5598.

Melcak, I., S. Melcakova, V. Kopsky, J. Vecerova, and I. Raska. 2001. Prespliceosomal assembly on microinjected precursor mRNA takes place in nuclear speckles. *Mol. Biol. Cell*. 12:393–406.

Misteli, T., J.F. Caceres, and D.L. Spector. 1997. The dynamics of a pre-mRNA splicing factor in living cells. *Nature*. 387:523–527.

Ossareh-Nazari, B., C. Maison, B.E. Black, L. Levesque, B.M. Paschal, and C. Dargemont. 2000. RanGTP-binding protein NXT1 facilitates nuclear export of different classes of RNA in vitro. *Mol. Cell. Biol.* 20:4562–4571.

Reed, R., and E. Hurt. 2002. A conserved mRNA export machinery coupled to pre-mRNA splicing. *Cell*. 108:523–531.

Rodrigues, J.P., M. Rode, D. Gatfield, B.J. Blencowe, M. Carmo-Fonseca, and E. Izaurralde. 2001. REF proteins mediate the export of spliced and unspliced mRNAs from the nucleus. *Proc. Natl. Acad. Sci. USA*. 98:1030–1035.

Shopland, L.S., C.V. Johnson, and J.B. Lawrence. 2002. Evidence that all SC-35 domains contain mRNAs and that transcripts can be structurally constrained within these domains. *J. Struct. Biol.* 140:131–139.

Smith, K.P., P.T. Moen, K.L. Wyder, J.R. Coleman, and J.B. Lawrence. 1999. Processing of endogenous pre-mRNAs in association with SC-35 domains is gene specific. *J. Cell Biol.* 144:617–629.

Spector, D.L. 1990. Higher order nuclear organization: three-dimensional distribution of small nuclear ribonucleoprotein particles. *Proc. Natl. Acad. Sci. USA*. 87:147–151.

Spector, D.L., X.D. Fu, and T. Maniatis. 1991. Associations between distinct pre-mRNA splicing components and the cell nucleus. *EMBO J.* 10:3467–3481.

Stanek, D., T. Kiss, and I. Raska. 2000. Pre-ribosomal RNA is processed in permeabilised cells at the site of transcription. *Eur. J. Cell Biol.* 79:202–207.

Svitkina, T.M., and G.G. Borisy. 1999. Arp2/3 complex and actin depolymerizing factor/cofilin in dendritic organization and treadmilling of actin filament array in lamellipodia. *J. Cell Biol.* 145:1009–1026.

Wagner, S., S. Chiosea, M. Ivshina, and J.A. Nickerson. 2004. In vitro FRAP reveals the ATP-dependent nuclear mobilization of the exon junction complex protein SRm160. *J. Cell Biol.* 164:843–850.

Weil, D., S. Boutain, A. Audibert, and F. Dautry. 2000. Mature mRNAs accumulated in the nucleus are neither the molecules in transit to the cytoplasm nor constitute a stockpile for gene expression. *RNA*. 6:962–975.

Zhou, Z., M.J. Luo, K. Straesser, J. Katahira, E. Hurt, and R. Reed. 2000. The protein Aly links pre-messenger-RNA splicing to nuclear export in metazoans. *Nature*. 407:401–405.

Zirbel, R.M., U.R. Mathieu, A. Kurz, T. Cremer, and P. Lichter. 1993. Evidence for a nuclear compartment of transcription and splicing located at chromosome domain boundaries. *Chromosome Res.* 1:93–106.